RESEARCH ARTICLE

Equivalent Modeling and Typical Scenario Screening of Wind Farms for the Stability Control Strategy Verification

Xijian Dong[1,*], Jialong Wu[1], Yuqi Ma[1], Jiaqi Feng[1], Yajie Li[1], Ming Lei[1] and Kui Deng[1]

[1] State Grid Electric Power Research Institute (NARI Group Corporation), Nanjing 211106, China

Abstract

This paper proposes a novel equivalent modeling framework for wind farms, specifically designed for the "grid simulation with physical security and stability control device" co-simulation environment. As the scope of stability control expands from the farm level to individual feeders and turbines, conventional equivalent models are inadequate for validating advanced strategies. To address this issue, a framework is proposed that integrates the architecture and operational principles of security and stability control systems. Within the scope of centralized renewable energy transmission grids, a technical route for equivalent modeling of wind farms that incorporates stability control actions is presented, adopting a five-machine equivalent method. Furthermore, a typical scenario selection method based on two-dimensional Kernel Density Estimation (2D-KDE) is developed, utilizing the active power recovery characteristics of the equivalent model. The efficacy of the proposed method is validated on an extended IEEE 10-machine 39-bus system.

Submitted: 29 June 2026
Revised: 07 August 2026
Accepted: 11 August 2026
Published: 24 August 2026

Vol. 2, **No.** 3, 2026.
10.62762/TSSR.2026.528149

***Corresponding author:**
✉ Xijian Dong
dong_xijian@163.com

Keywords: wind farms, stability control strategy verification, equivalent modeling, security and stability control system, typical scenario.

1 Introduction

Renewable energy strategies are actively driving the large-scale integration and deployment of wind power [1]. However, the inherent characteristics of wind power generation—including low inertia, minimal damping, and limited voltage support—introduce complex stability issues and heighten the risk of cascading failures following system faults [2, 3]. Consequently, the secure and stable operation of modern power grids relies heavily on security and stability control systems. The rigorous validation of these systems is a critical prerequisite for maintaining grid reliability.

The verification of security and stability control systems entails multi-level and multi-dimensional testing. Under laboratory conditions, the prevalent methodology is the "grid simulation with physical security and stability control device" co-simulation approach, which is employed to confirm the precision, efficacy, and logical correctness of stability control strategies [4, 5]. However, practical constraints often necessitate the simplification of power grid components and topologies. Wind farms, serving as primary control objects, possess distinct dynamic characteristics that profoundly influence control switching and protection mechanisms during grid

Citation
Dong, X., Wu, J., Ma, Y., Feng, J., Li, Y., Lei, M., & Deng, K. (2026). Equivalent Modeling and Typical Scenario Screening of Wind Farms for the Stability Control Strategy Verification. *ICCK Transactions on Systems Safety and Reliability*, 2(3), 207–219.

disturbances. The primary challenge lies in developing a realistic modeling method for these wind farms to effectively validate stability control strategies.

The equivalent modeling of wind farms is generally classified into single-machine and multi-machine equivalence [6–8]. While single-machine equivalence simplifies a wind farm into a single equivalent unit, it is particularly inadequate for large-scale installations due to significant variations in individual unit operating conditions caused by wake and hysteresis effects. This oversimplification can lead to substantial equivalent errors in transient stability simulation analyses [9].

The multi-machine equivalence approach mitigates this by simplifying a wind farm into multiple representative units [10, 11]. In [12–14], real-time indicators such as active power and short-circuit current during faults are selected as clustering criteria. Although these high-dimensional indicators can enhance simulation accuracy, they require complex data processing and clustering algorithms, hindering their application in engineering practice. Conversely, methods proposed in [15, 16] utilize post-fault information, such as rotational speed, active/reactive power, terminal voltage, and virtual power angle, to analyze power system stability. While effective for fault inversion, these methods are limited in verifying stability control strategies based on anticipated faults, as they rely on data collected post-disturbance. Alternatively, scenario-based methods introduced in [17, 18] utilize the pre-fault initial wind speed of each unit as known data. This approach is highly applicable in engineering contexts and facilitates the effective simulation verification of stability control strategies for potential faults.

As wind farms expand in scale, the traditional “whole-farm switching” approach to stability control becomes less economically viable and logically rational. Modern security and stability control systems have transitioned towards more granular “feeder-level” or “turbine-level” control strategies. However, existing wind farm equivalent methods inadequately address the efficacy of equivalent models when specific turbines are tripped as a result of stability control actions. There is a critical need for an equivalent method that explicitly considers the impact of stability control actions.

This paper proposes an effective equivalent modeling framework that integrates the architecture and operational principles of security and stability control systems. Within this framework, a five-machine equivalent method that accounts for stability control actions is introduced. Additionally, this paper presents a wind farm typical scenario screening method based on the active power recovery attributes of the equivalent model, providing robust support for scenario generation in wind farm studies.

The remainder of this paper is organized as follows: Section 2 proposes the equivalent modeling framework considering stability control actions. Section 3 details the active power equivalent error analysis and the proposed equivalent method for wind farms. Section 4 describes the typical scenario screening methodology for stability control verification. Section 5 presents the method verification to demonstrate the efficacy of the proposed approach.

2 Equivalent Modeling Framework Considering Stability Control Actions

The security and stability control system typically comprises a control master station, control substations, and execution stations [19]. The wind farm execution station plays a pivotal role by receiving active power control commands (P_{ord}) from superior stability control devices. Its primary function is to sequentially trip feeders or turbines based on a predefined priority. Concurrently, it must ensure that the sum of the pre-fault steady-state active power of the tripped turbines meets or exceeds P_{ord}. In other words, the actual tripped active power (P_{cut}) must satisfy $P_{\text{cut}} \geq P_{\text{ord}}$. The value of P_{cut} is subsequently reported back to the control master station.

Traditional wind farms typically employ a “whole-farm switching” control strategy. As security and stability control systems extend their control scope to lower voltage levels, wind farms now predominantly utilize a “feeder-level” control strategy, with panoramic monitoring systems even enabling “turbine-level” control. Both “whole-farm switching” and “feeder-level” strategies can be considered as aggregated applications of the more granular “turbine-level” control logic, as they ultimately result in the tripping of individual turbines. Therefore, the analysis of the equivalent modeling framework for wind farms, considering stability control actions, adopts the “turbine-level” control strategy as the representative framework.

In a wind farm scenario, turbines are grouped by wind speed, with each cluster aggregated into a single equivalent turbine. To ensure the resulting equivalent model is suitable for use within security and stability control system verification environments—where model complexity must be balanced against computational efficiency [20]—the equivalent turbine's active power output typifies the average power of the entire cluster, and its equivalent wind speed is calculated as:

$$v_{\mathrm{eq}} = f^{-1}\left(\frac{1}{N}\sum_{i=1}^{N} f(v_i)\right) \tag{1}$$

where v_{eq} is the equivalent wind speed for a single equivalent turbine, N is the number of turbines in the cluster, $f(v_i)$ is the power-wind speed characteristic function of a turbine, and v_i is the wind speed of the i-th turbine.

The response time of stability control systems is typically on the order of hundreds of milliseconds [21], whereas the active power response of wind farms exhibits a considerably slower time scale compared to the stability control action, as the aggregated output power adjusts gradually following wind speed variations—a characteristic that must be preserved in equivalent modeling [22]. Therefore, it can be assumed that the wind speed of each turbine remains constant following a stability control action, and the clustering results remain unchanged.

However, the stability control action results in a portion of the turbines being tripped. Consequently, it is imperative to adjust the equivalent turbine multiplier to accurately reflect this action. The formula for calculating the updated equivalent turbine multiplier is (2).

$$\begin{cases} n = N, & t < t_{\mathrm{k}} \\ n' = \dfrac{\sum\limits_{i\in S} f(v_i)}{f(v_{\mathrm{eq}})}, & t \geq t_{\mathrm{k}} \end{cases} \tag{2}$$

where n is the equivalent turbine multiplier post-action, t_{k} is the timing of the stability control action, and S is the set of turbines retained within the cluster after the action. The superscript denotes the state after the stability control action.

Following the stability control action, the topological structure of the wind farm changes, leading to corresponding variations in power losses within the collection lines. To maintain a constant steady-state active power loss before and after equivalence—a standard principle in wind farm equivalent modeling [6] that must also comply with the grid connection requirements [23]—the equivalent length of the collection line is calculated as:

$$\begin{cases} l_{\mathrm{eq}} = \dfrac{\sum\limits_{i=1}^{N}\left(l_i \cdot P(l_i)^2\right)}{\left(\sum\limits_{i=1}^{N} p_i\right)^2}, & t < t_{\mathrm{k}} \\ l'_{\mathrm{eq}} = \dfrac{\sum\limits_{i=1}^{N}\left(l_i \cdot P'(l_i)^2\right)}{\left(\sum\limits_{i=1}^{N} p'_i\right)^2}, & t \geq t_{\mathrm{k}} \end{cases} \tag{3}$$

where l_{eq} is the equivalent length of the collector line, l_i is the length of the collector line associated with the i-th turbine, $P(l_i)$ is the steady-state active power flowing through collector line l_i, and p_i is the steady-state active power generated by the i-th turbine. It is important to note that if the i-th turbine is tripped off following stability control, p'_i is rendered zero.

3 Equivalent Method for Wind Farms

3.1 Error Analysis Considering Stability Control Action

During a deep voltage dip at the point of common coupling (PCC) of a wind farm, it is required to provide reactive power support for voltage recovery, and active power should be restored after fault clearing in accordance with grid code requirements [24, 25]. The reactive response of the turbines during low-voltage ride-through is a function of the control strategy, terminal voltage, and pre-fault steady-state Q_0 (normally zero). In multi-machine equivalent models, the reactive characteristics of turbine clusters under fault conditions can be represented by an aggregate equivalent, as the reactive behavior is primarily governed by the shared control logic and the common bus voltage [26]. The same control strategies and similar voltages among turbines during deep dips cause minor differences in reactive responses. However, due to the complicated operating conditions of wind farms, significant differences exist in the active power responses, which motivates this work to perform error analysis on the active power.

Equivalent modeling can be categorized into single-machine and multi-machine equivalence, with the latter essentially comprising multiple single-machine equivalents [27]. Consequently, the analysis of active power equivalent errors, considering the stability control action, is based on the single-machine equivalence.

For relatively low voltage drops, the active power recovery of wind farms is brief, and stability control

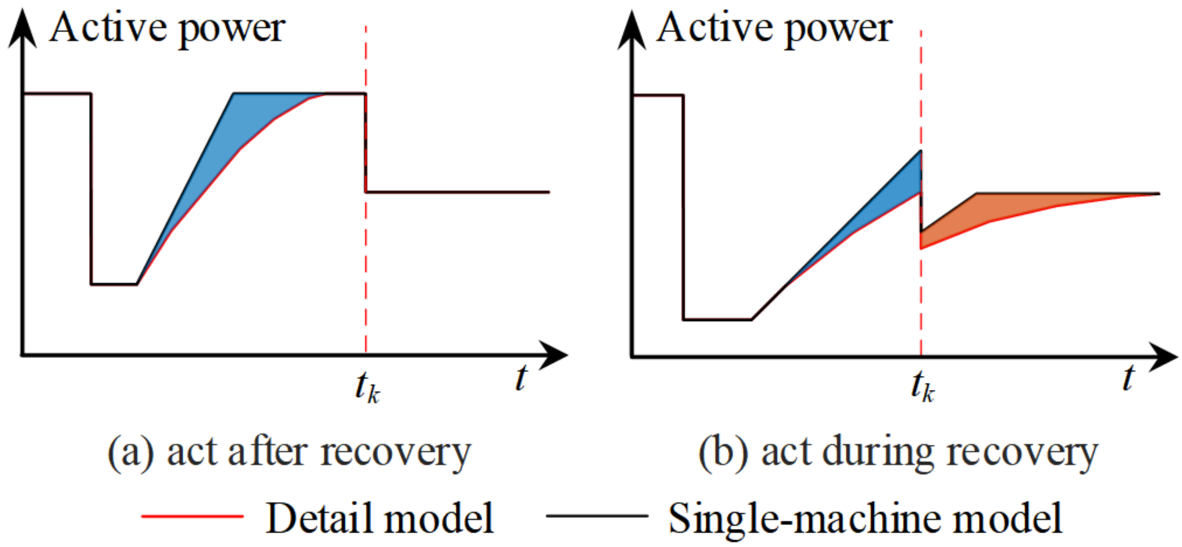

Figure 1. Equivalent error in active power of wind farms considering stability control actions.

may act after this recovery, as depicted in Figure 1(a). Conversely, for more significant voltage drops, this process is prolonged, and stability control may act during the recovery period, as illustrated in Figure 1(b).

When stability control acts after active power recovery, the active power equivalent error of single-machine model is given by (4) disregarding the error during the fault period.

$$e(t) = \begin{cases} p(t) \cdot \alpha(t) - P_\alpha(t), & t_c < t < t_\mathrm{k} \\ 0, & t \geq t_\mathrm{k} \end{cases} \tag{4}$$

where $e(t)$ is the equivalent error of active power in the single-machine model, $p(t)$ is the active power of the turbine in the recovery period at time t, $\alpha(t)$ is the number of turbines in the farm that have completed active power recovery at time t, $P_\alpha(t)$ is the total steady-state active power of the α turbines at time t and t_c is the time of fault removal.

When stability control acts during active power recovery, the single-machine model's active power equivalent error is given by (5).

$$e(t) = \begin{cases} p(t) \cdot \alpha(t) - P_\alpha(t), & t_c < t < t_\mathrm{k} \\ [p(t) \cdot \alpha(t) - P_\alpha(t)] + [p(t) \cdot (n' - n_c)], & t \geq t_\mathrm{k} \end{cases} \tag{5}$$

where n_c is the number of turbines retained after the stability control action in the farm.

For brevity, $[p(t) \cdot \alpha(t) - P_\alpha(t)]$ and $[p(t) \cdot (n' - n_c)]$ are denoted as e_1 and e_2. Thus, the active power equivalent error considering the stability control action is given in (6).

$$e = \begin{cases} e_1, & t_c < t < t_\mathrm{k} \\ e_1 + e_2, & t \geq t_\mathrm{k} \,\&\, t < t_\mathrm{end} \\ 0, & t \geq t_\mathrm{k} \,\&\, t \geq t_\mathrm{end} \end{cases} \tag{6}$$

3.1.1 e_1 *analysis*

e_1 is the error caused by the equivalent model treating the turbines that have completed active power recovery as being in the recovery period. This error is primarily related to the difference between $p(t) \cdot \alpha(t)$ and $P_\alpha(t)$. When the number of clusters increases, the difference between $p(t) \cdot \alpha(t)$ and $P_\alpha(t)$ within the same cluster becomes smaller, resulting in a smaller e_1.

The optimal clustering method, which minimizes the active power equivalent error for a specified number of clusters, was employed on the power farm. This was done to evaluate the error e_1 associated with varying numbers of clusters, as depicted in Figure 2. It was observed that as the number of clusters rose, the error e_1 exponentially diminished. A notable reduction in error e_1 was evident when transitioning from single-machine equivalence to two-machine equivalence.

3.1.2 e_2 *analysis*

e_2 results from the discrepancy between the equivalent machine multiplication value n' and the actual unit count n_c. This discrepancy is fundamentally caused by the stability control action, with the difference between n' and n_c mainly determined by the composition of the tripped turbines.

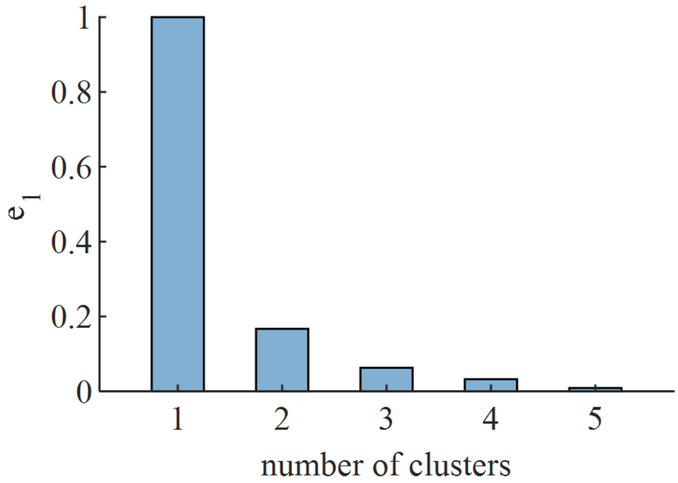

Figure 2. e_1 with different numbers of clusters.

Figure 3 illustrates the influence of e_2 on the overall e, which is analyzed as described below:

(1) When $e_2 > 0$, e is positive and decreases as e_2 diminishes;

(2) When $e_2 < 0$, the error caused by e_2 partially offsets the equivalent error caused by e_1;

(3) After reaching its minimum value, e begins to increase in the opposite direction.

e becomes significant when e_2 is either sufficiently large or small. To quantify the effect of e_2 on e when e_2 is sufficiently large or small, the active power error area without stability control serves as the reference. For $t > t_{\mathrm{k}}$, the error areas with and without stability control are compared, as shown in Figure 4.

Let r represent the ratio of active power error areas with and without stability control for $t > t_{\mathrm{k}}$, as in (7). If $r > 1$, stability control action expands the active power error areas compared to its inaction.

$$r = \frac{S_\gamma}{S_{\gamma'}} \tag{7}$$

where $S_{\gamma'}$ is the active power error area without stability control actions and S_γ is the active power error area with stability control actions.

Next, simulations are employed to assess whether r could exceed 1. The setup involves a 10-turbine wind farm with 50 randomly generated operating scenarios, covering uniform and non-uniform wind speed distributions. For each scenario, 100 turbine-tripping cases are tested, including combinations of 1 to 10 turbines tripped and varying actual tripped active power (P_{cut}) for the same number of turbines tripped.

In this study, $r_{\max}$ denotes the maximum r across 100 turbine-tripping cases, with statistical results shown in Figure 5. For the randomly generated 100 turbine-tripping cases, the $r_{\max}$ of each scenario exceeds 1, with a maximum $r_{\max}$ of 3.28, a minimum $r_{\max}$ of 1.36, and an average $r_{\max}$ of 1.69. These findings indicate that stability control actions may indeed lead to an increase in the active power error.

Statistical analysis reveals that cases with $r > 1$ mainly involve tripping low-wind-speed turbines. The reasons are as follows:

The number of remaining turbines n_c in the wind farm after stability control can be expressed as:

$$n_c = \frac{\sum_{i \in S} f(v_i)}{f(v_{\mathrm{eqc}})} \tag{8}$$

where v_{eqc} represents the equivalent wind speed of the retained turbines after stability control action.

The difference between n' and n_c can be expressed as:

$$n' - n_c = \sum_{i \in S} f(v_i) \cdot \left(\frac{1}{f(v_{\mathrm{eq}})} - \frac{1}{f(v_{\mathrm{eqc}})} \right) \tag{9}$$

When low-wind-speed turbines are tripped, $v_{\mathrm{eq}} < v_{\mathrm{eqc}}$, thus according to (9), $(n' - n_c) > 0$, leading to $e_2 > 0$. Meanwhile, retaining high-wind-speed turbines prolongs active power recovery, leading to an increase in the cumulative error represented by e_2. Consequently, this results in a larger active power error when stability control actions are considered.

3.2 Clustering Method

Based on the relationship between active power and rotor speed, wind turbines operate in three distinct regions: start-up, Maximum Power Point Tracking (MPPT), and constant speed/power [28]. The differing control strategies in these regions result in unique active power responses.

In [16], the single-machine error remains notably small in the start-up and constant speed/power regions but significantly increases in the MPPT region. Since most wind turbines operate in the MPPT region during normal wind farm operation, a multi-machine equivalent approach is essential to minimize the active power equivalent error.

Firstly, the optimal two-machine clustering method in the MPPT region is determined to minimize e_1. Assuming there are m turbines in the MPPT region,

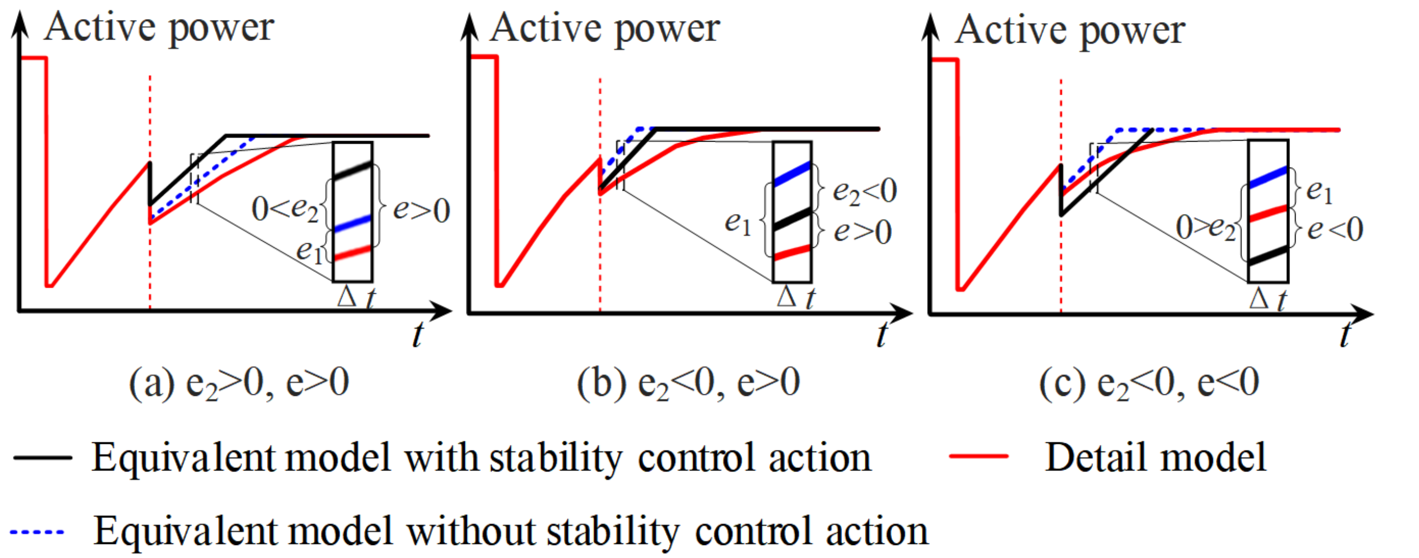

Figure 3. The influence of e_2 on the overall e.

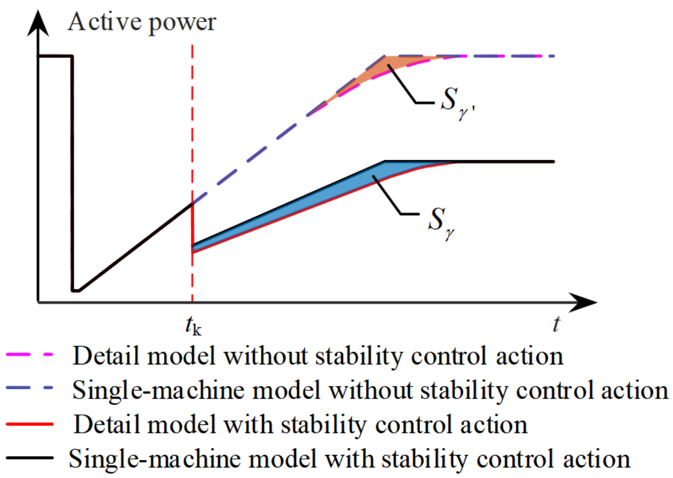

Figure 4. Error areas between stability control action and inaction in a single-machine equivalent model.

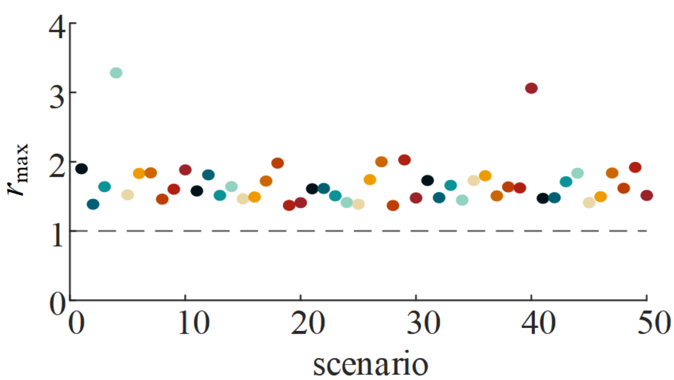

Figure 5. r_{max} under 100 random generator tripping combinations across different scenarios.

their corresponding steady-state active power outputs are $\boldsymbol{p} = \{p_1, p_2, \ldots, p_m\}$. The relationship of active power response among the single-machine model, two-machine model, and detailed model is illustrated in Figure 6.

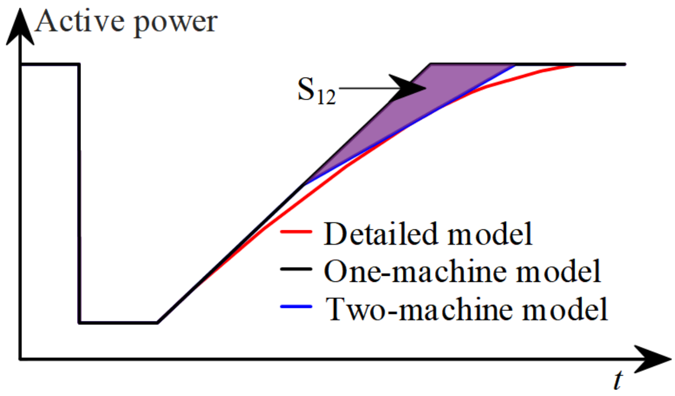

Figure 6. Active power response without stability control action in detailed and equivalent models.

In the two-machine model, different clustering methods yield different active power errors. Given that the active power error of the single-machine model is fixed, to minimize the active power error of the two-machine model, it is necessary to maximize the active power error between the single-machine model and the two-machine model. This is equivalent to maximizing the area of the purple triangular region, as shown in (10).

$$\max S_{12} = S_1 - S_2 \tag{10}$$

where S_{12} is the error area enclosed by the active power response curves of the single-machine model and the two-machine model, S_1 is the active power error area of the single-machine model and S_2 is the active power error area of the two-machine model.

The steady-state active power split point p_{div} serves to divide the MPPT area's m turbines into two distinct clusters. The cluster characterized by a lower average power is designated as Group A, while the cluster with a higher average power is referred to as Group B, thus satisfying:

$$\begin{cases} \sum_{i=1}^{m} p_i = p_{\text{mean}}^A \cdot n_A + p_{\text{mean}}^B \cdot n_B \\ p_{\text{mean}}^A \leq p_{\text{mean}}^B \end{cases} \tag{11}$$

where p_{mean}^A and p_{mean}^B are the steady-state average active power of Group A and Group B, n_A is the number of turbines in Group A and n_B is the number of turbines in Group B. n_A and n_B satisfy the following relationship:

$$m = n_A + n_B \tag{12}$$

Assuming the active power recovery slope of each turbine is k_u, then:

$$\begin{cases} t_A = p_{\text{mean}}^A / k_u \\ t_B = p_{\text{mean}}^B / k_u \\ t_s = p_{\text{mean}} / k_u \end{cases} \tag{13}$$

where t_A and t_B are the active power recovery durations for Group A and Group B, t_s is the active power recovery duration for the single-machine model, satisfying $t_A \leq t_s \leq t_B$, and p_{mean} is the average active power before the fault in the MPPT region, satisfying (14).

$$p_{\text{mean}} = \frac{1}{m} \sum_{i=1}^{m} p_i \tag{14}$$

The area S_{12} is given by (15).

$$S_{12} = \frac{1}{2} \left(\sum_{i=1}^{m} p_i - m p_{\text{mean}}^A \right) (t_B - t_s) \tag{15}$$

By substituting (13) into (15), (16) is derived.

$$S_{12} = \frac{1}{2k_u} \left(\sum_{i=1}^{m} p_i - m p_{\text{mean}}^A \right) (p_{\text{mean}}^B - p_{\text{mean}}) \tag{16}$$

By substituting (14) into (16) and expanding, (17) is obtained.

$$S_{12} = \frac{1}{2k_u} \left[\sum_{i=1}^{m} p_i \cdot (p_{\text{mean}}^A + p_{\text{mean}}^B) - m p_{\text{mean}}^A p_{\text{mean}}^B - m p_{\text{mean}}^2 \right] \tag{17}$$

Given that k_u, p_{mean}, and m are constant values, the maximization of S_{12} can be achieved by (18).

$$\max \sum_{i=1}^{m} p_i \cdot (p_{\text{mean}}^A + p_{\text{mean}}^B) - m p_{\text{mean}}^A p_{\text{mean}}^B \tag{18}$$

Finally, through the incorporation of (11) and (12) into (18), the following result is obtained.

$$\max (p_{\text{mean}}^A)^2 \cdot n_A + (p_{\text{mean}}^B)^2 \cdot n_B \tag{19}$$

The steady-state active power split point p_{div}, corresponding to p_{mean}^A and p_{mean}^B in (19), represents the optimal split point for the two-machine model in the MPPT region. This minimizes the active power error of the two-machine model in the MPPT region. This active power split point p_{div} is denoted as $p_{\text{div1}}^{\text{MPPT}}$.

To mitigate the significant active power error e caused by e_2 when tripping low-wind-speed turbines, this paper proposes secondary clustering for the higher-average-power machine group in the MPPT region. The steady-state active power split point is set as the cluster's steady-state average active power, as shown in (20).

$$p_{\text{div2}}^{\text{MPPT}} = p_{\text{mean}}^B \tag{20}$$

In summary, this section proposes a five-machine clustering method for wind farms considering stability control actions. First, all turbines in a wind farm are grouped into three clusters based on the start and end wind speeds in the MPPT region. Then, the MPPT region is further divided into three clusters using steady-state active power split points $p_{\text{div1}}^{\text{MPPT}}$ and $p_{\text{div2}}^{\text{MPPT}}$, achieving the five-machine clustering. The methodology is illustrated in Figure 7.

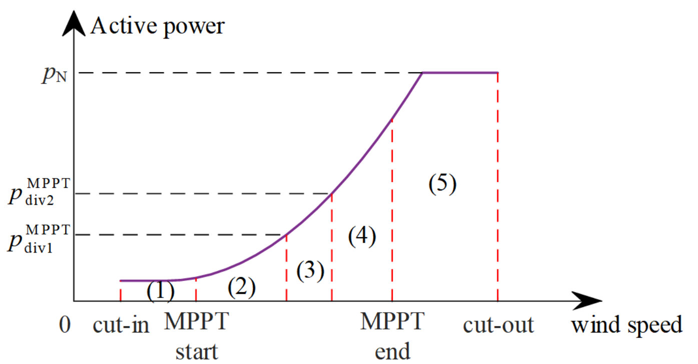

Figure 7. Schematic diagram of the five-machine equivalent strategy.

4 Wind Farm Typical Scenarios Screening for Stability Control Verification

4.1 Typical Scenario Definition

The verification of stability control strategies is conducted based on the typical operating conditions of the power system, where the steady-state active power of the wind farm is determined. Therefore, the typical scenario of the wind farm $\zeta^* = (v_1^*, v_2^*, \cdots, v_M^*)$ must satisfy the following condition:

$$\sum_{i=1}^{M} f(v_i^*) = P_{\text{obj}} \tag{21}$$

where P_{obj} is the target active power in the steady state, and M is the number of turbines in the wind farm.

The verification of stability control strategies is based on system stability. Wind farms affect stability through their active power response. In different scenarios, with the same steady-state active power P_{obj}, the recovery characteristics of a wind farm after fault may be different, resulting in different effects on system stability. Therefore, it is necessary to select a typical scenario with representative active power recovery characteristics.

The active power recovery characteristic of a wind farm's equivalent model depends on the number of equivalent machines. For a single-machine model ($N_{\text{eq}} = 1$), these characteristics are consistent across all operating scenarios, as shown in Equation (22), making any scenario representative of all others.

$$P(t) = k_u M(t - t_{\text{cqs}}) + P_{\text{obj}}, t_c < t < t_{\text{cqs}} \tag{22}$$

where t_{cqs} is the steady-state time after fault clearance for single-machine model.

As the number of equivalent machines (N_{eq}) increases, the differences in active power recovery characteristics across scenarios grow, peaking at $N_{\text{eq}} = M$. Thus, this paper defines the typical scenario ζ^* for stability control validation with representative active power recovery characteristics based on the five-machine equivalent model ($N_{\text{eq}} = 5$).

4.2 Typical Scenario Selection Method Based on 2D-KDE

4.2.1 Data preprocessing

In a wind farm with M turbines, each scenario represents the wind speeds of all turbines at a specific moment, with W total scenarios, as illustrated in (23) and (24). The initial scenario set Φ_0 has a dimension of $W \times M$.

$$\Phi_0 = (\zeta_1, \zeta_2, \cdots, \zeta_k, \cdots, \zeta_W)^{\text{T}} \tag{23}$$

$$\zeta_k = (v_{k,1}, v_{k,2}, \cdots, v_{k,M}) \tag{24}$$

where W is the number of the initial scenarios, which is collected by SCADA system of the wind farm.

The active power of the wind farm under different scenarios is represented as discrete data points as shown in (25).

$$\Omega = \{P_{\zeta_k} \mid P_{\zeta_k} = \sum_{i=1}^{M} f(v_{k,i}), k = 1, 2, \cdots, W\} \tag{25}$$

where P_{ζ_k} is the steady-state active power for the k-th scenario.

Nevertheless, the quantity of scenarios that align with the target power value P_{obj} is finite and might even be non-existent. Consequently, scenarios situated within the interval $(P_{\text{obj}} - \delta, P_{\text{obj}} + \delta)$ are chosen from Ω for data preprocessing.

Let the rated power of the turbine be p_n and the scaling factor for k-th scenario be α_k. The scaled power $p_{i,k}$ of the i-th turbine satisfy (26) and (27).

$$p'_{i,k} = \min(\alpha_k \cdot f(v_{i,k}), p_n) \tag{26}$$

$$\sum_{i=1}^{M} p'_{i,k} = P_{\text{obj}} \tag{27}$$

Thus, the scaling factor α_k should satisfy (28).

$$\sum_{i=1}^{M} \min(\alpha_k \cdot f(v_{i,k}), p_n) = P_{\text{obj}} \tag{28}$$

Due to the nonlinearity in (28), direct solution is complex. This paper employs an iterative method, where the value of α_k varies in each iteration. Consequently, α_k is no longer a specific numerical value but rather a set of vectors, as expressed in (29):

$$\alpha_k = \{\alpha_{k,0}, \alpha_{k,1}, \cdots, \alpha_{k,z}, \cdots, \alpha_{k,\text{end}}\} \tag{29}$$

The formula for $\alpha_{k,z}$ is defined as:

$$\alpha_{k,z} = \begin{cases} \dfrac{P_{\text{obj}}}{\sum\limits_{i=1}^{M} f(v_{k,i})}, & z = 0 \\ \dfrac{P_{\text{h}} - N_{\text{h}} \cdot p_n}{P_{\text{obj}} - P_{\text{h}}}, & z \geq 1 \end{cases} \tag{30}$$

where P_{h} is the total active power of abnormal turbines exceeding p_n and N_{h} is the number of abnormal turbines exceeding p_n. The loop ends when $P_{\text{h}} = 0$. The scenario set after data preprocessing is denoted as $\Phi_1 = (\zeta'_1, \zeta'_2, \cdots, \zeta'_{|\Phi_1|})^{\text{T}}$.

4.2.2 *Candidate scenario screening*

The steady-state active power division point p_{div} is chosen to maximize (19), grouping all wind farm units accordingly.

Let the parameters of the first equivalent machine be $v_{\text{eq1}}^{(2)}$ and $n_1^{(2)}$, and those of the second equivalent machine be $v_{\text{eq2}}^{(2)}$ and $n_2^{(2)}$. These four features are interdependent, constrained by (31) and (32), resulting in only two independent features.

$$f(v_{\text{eq1}}^{(2)}) \cdot n_1^{(2)} + f(v_{\text{eq2}}^{(2)}) \cdot n_2^{(2)} = P_{\text{obj}} \tag{31}$$

$$n_1^{(2)} + n_2^{(2)} = M \tag{32}$$

$v_{\text{eq2}}^{(2)}$ and $n_2^{(2)}$ are selected as the features T for candidate scenario screening.

$$T = [v_{\text{eq2}}^{(2)}, n_2^{(2)}] \tag{33}$$

The feature matrix Z_1 corresponding to different scenarios is:

$$Z_1 = \left[T_1, T_2, \cdots, T_{|\Phi_1|}\right]^{\text{T}} \tag{34}$$

Using the feature matrix Z_1 as input, the two-dimensional kernel density estimation algorithm computes the probability density values for all samples in the scenario set Φ_1. Scenarios with densities exceeding ε form the candidate set $\Phi_2 \subset \Phi_1$, as defined in (35).

$$\Phi_2 = \{\zeta_i' \mid f_1(T_i) > \varepsilon\} \tag{35}$$

where $f_1(T_i)$ is the probability density of scenario ζ_i'.

4.2.3 *Typical scenario identification*

Based on Section 3, the wind farm is equivalently represented by five machines, with parameters $(v_{\text{eq}}^{(i)}, n_i^{(i)})$ for the first, up to $(v_{\text{eq}}^{(5)}, n_5^{(5)})$ for the fifth. The key distinction between the five-machine and two-machine equivalents lies in the higher wind speed cluster of the five-machine model. The features for typical scenario identification are shown in (36).

$$G = \left[\max v_{\text{eqi}}^{(5)}, n_{\arg\max v_{\text{eqi}}}^{(5)}\right] \tag{36}$$

where i ranges from 1 to 5.

The feature matrix Z_2 corresponding to different scenarios is:

$$Z_2 = \left[G_1, G_2, \cdots, G_{|\Phi_2|}\right]^{\text{T}} \tag{37}$$

Using the feature matrix Z_2 as input, the 2D-KDE algorithm computes the probability density values for all samples in the scenario set Φ_2. The scenario with the highest density value is selected as the typical scenario ζ^*, as shown in (38).

$$\zeta^* = \arg\max_{\zeta_i \in \Phi_2} f_2(G_i) \tag{38}$$

where $f_2(G_i)$ is the probability density of scenario ζ_i.

4.3 Extreme scenario augmentation

The stability control strategy must be adaptable to both typical and extreme wind farm scenarios. Increasing the active power recovery time enhances the positive effect under a constant wind power output. The active power recovery time should be minimized in extreme scenarios, and the recovery time across different scenarios is determined by the wind turbine with the maximum wind speed. Therefore, in extreme scenarios, the wind speed for each wind turbine is:

$$v_i = f^{-1}\left(\frac{P_{\text{obj}}}{M}\right), i = 1, 2, \cdots, M \tag{39}$$

5 Method Verification

The effectiveness of the proposed five-machine equivalent method is verified using a simulation system constructed in PSCAD/EMTDC. The system includes 32 turbines, each with 6.25 MW, connected to Bus 19 of the IEEE-39 system, as shown in Figure 8.

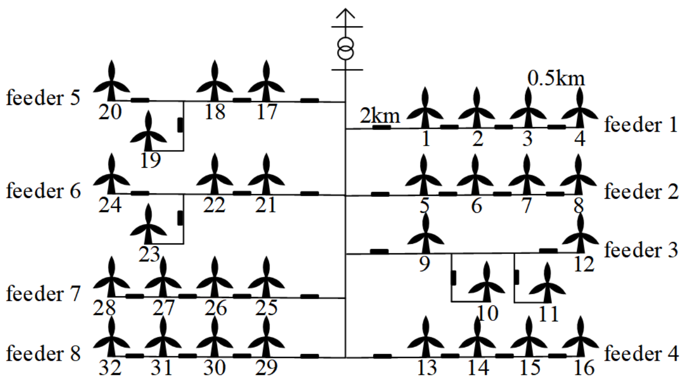

Figure 8. Wind farm topology.

The stability control action is simulated using manually set pulse triggers, emulating the "grid simulation & security and stability control device physical" approach for validating stability control strategies. The priority of each turbine is randomly assigned.

Set $P_{\text{obj}} = 145$ MW and determine the scenario ζ^* using Section 4 (wind speeds in Table 1).

Table 1. Typical scenario of $P_{obj} = 145$ MW.

Turbine	Wind speed/(m/s)
1∼8	6.92,8.24,8.63,10.03,6.92,8.25,8.67,9.84
9∼16	6.70,8.20,8.54,9.40,7.19,7.99,8.98,9.87
17∼24	8.38,8.08,9.02,8.39,8.38,10.03,9.12,8.50
25∼32	8.08,9.58,9.17,10.03,6.99,8.29,8.75,9.85

A three-phase short circuit at Bus 19 occurs at 12 s, lasting 0.625 s. To evaluate the equivalence accuracy of the proposed method considering the stability control action, two cases are configured as follows:

Case 1: voltage drops to 0.1 p.u., $P_{ord} = 50$ MW;

Case 2: voltage drops to 0.4 p.u., $P_{ord} = 30$ MW;

The proposed equivalent method is compared with single-machine and four-machine equivalents (using MPPT region start/end points and equivalent wind speeds of MPPT turbines). Since traditional single-machine and four-machine equivalents do not consider the stability control action, they must be integrated with the equivalent modeling framework described in Section 2. The simulation results of active power response for different models under two cases are presented in Figure 9.

When the stability control action is initiated ($t = 14$ s), all equivalent models can effectively characterize the instantaneous active power drop, demonstrating the rationality of the wind farm equivalent modeling framework considering stability control actions proposed in Section 2.

After the stability control action ($t > 14$ s), the proposed model effectively characterizes the active power recovery process, with recovery times closely matching the detailed model. As shown in Table 2, the proposed model significantly outperforms the four-machine model in terms of both MAPE and maximum error across all cases, reducing the MAPE by approximately 67% in Case 1 and 57% in Case 2.

This suggests that the proposed model demonstrates superior adaptability across diverse validation scenarios compared to the four-machine model.

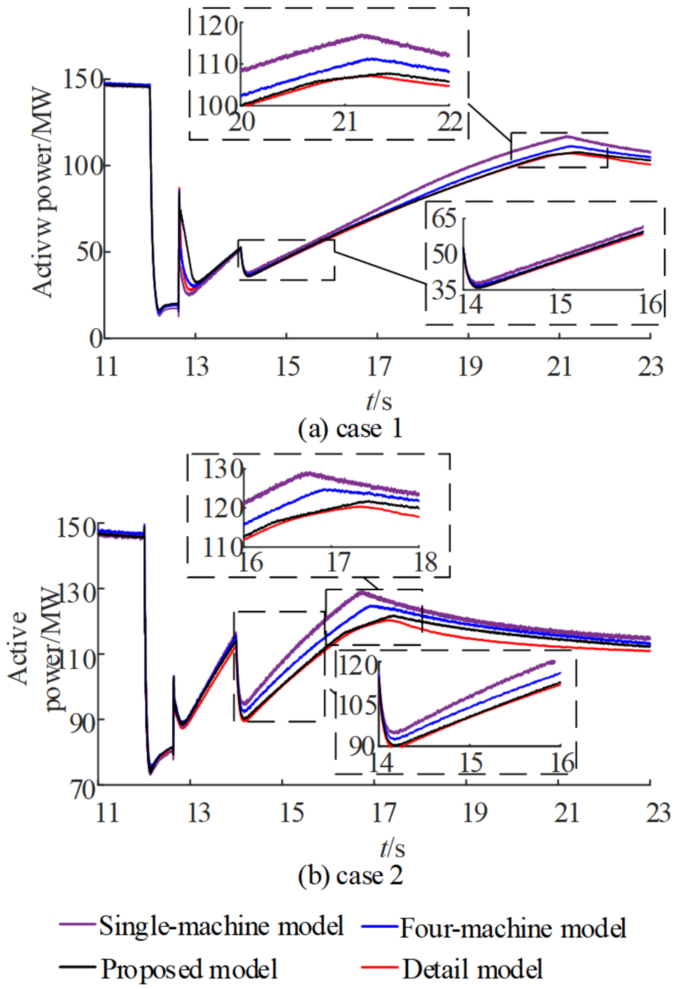

Figure 9. Active power response for different models under two cases.

6 Conclusion

This paper proposes an equivalent modeling method for large-scale wind farms considering stability control actions, as well as a typical scenario selection method. Together, they provide a highly practical engineering solution for renewable energy station equivalent modeling and typical scenario selection in the verification of security and stability control strategies.

(1) The proposed equivalent method for large-scale wind farms, which accounts for stability control actions, groups wind turbines based on their wind speeds. The relevant indicators are observable and measurable, ensuring strong practical applicability in engineering. This method accurately reflects the station's response characteristics under "feeder-level" or "turbine-level" control modes and their actions. Furthermore, it provides key technical support for future, more refined stability control strategies, such as "generation modulation instead of tripping."

(2) The proposed typical scenario selection method based on 2D-KDE resolves the issue of selecting typical operational scenarios for renewable energy stations that are grouped and modeled based on wind speeds. It offers a viable approach for selecting typical scenarios from massive operational conditions

Table 2. Calculation results of key indicators for different equivalence methods.

	Case 1		Case 2	
	MAPE/%	maximum error /MW	MAPE/%	maximum error /MW
Single-machine model	7.14	10.09	5.48	11.41
Four-machine model	2.44	4.64	3.35	5.98
Proposed model	0.80	2.71	1.45	3.14

in practical simulation verification.

Considering the current development status of stability control technologies, the wind farm equivalent modeling and typical scenario selection methods proposed in this paper focus on preserving the active power response characteristics of the station. Future work will further consider reactive power response deviations to optimize the equivalent method. Additionally, exploration will be conducted into equivalent modeling technologies for renewable energy stations, which are tailored to verify control strategies for emerging stability issues, such as broadband oscillation.

Data Availability Statement

Data will be made available on request.

Funding

This work was supported by the Technical Research Service Project of SGCC under Grant SGZB0000GDJS2601136.

Conflicts of Interest

The authors are affiliated with the State Grid Electric Power Research Institute (NARI Group Corporation), Nanjing 211106, China. The authors declare that this affiliation had no influence on the study design, data collection, analysis, interpretation, or the decision to publish, and that no other competing interests exist.

AI Use Statement

The authors declare that no generative AI was used in the preparation of this manuscript.

Ethical Approval and Consent to Participate

Not applicable.

References

[1] Ahmed, S. D., Al-Ismail, F. S., Shafiullah, M., Al-Sulaiman, F. A., & El-Amin, I. M. (2020). Grid integration challenges of wind energy: A review. *IEEE Access*, *8*, 10857-10878. [CrossRef]

[2] Saleem, M. I., Saha, S., Roy, T. K., & Ghosh, S. K. (2024). Assessment and management of frequency stability in low inertia renewable energy rich power grids. *IET Generation, Transmission & Distribution*, *18*(7), 1372-1390. [CrossRef]

[3] Aljarrah, R., Fawaz, B. B., Salem, Q., Karimi, M., Marzooghi, H., & Azizipanah-Abarghooee, R. (2024). Issues and challenges of grid-following converters interfacing renewable energy sources in low inertia systems: A review. *IEEE Access*, *12*, 5534-5561. [CrossRef]

[4] State Administration for Market Regulation, & Standardization Administration of China. (2024). *Inspection specification for security and stability control system of power system* (GB/T 22384-2024). Retrieved from https://codeofchina.com/standard/GBT22384-2024.html

[5] He, J., Xu, H., Liu, Q., & Ren, J. (2024, October). Unified Simulation and Verification Technology for Primary and Secondary Control in Power Systems Based on Digital Stability Control System. In *2024 IEEE PES 16th Asia-Pacific Power and Energy Engineering Conference (APPEEC)* (pp. 1-5). IEEE. [CrossRef]

[6] Zou, J., Peng, C., Yan, Y., Zheng, H., & Li, Y. (2014). A survey of dynamic equivalent modeling for wind farm. *Renewable and Sustainable Energy Reviews*, *40*, 956-963. [CrossRef]

[7] Uddin, M. H., Khalid, J., Smailes, M., Liang, J., & Wang, S. (2026). Accurate and computationally efficient aggregated modelling of offshore wind farms for grid compliance. *IEEE Transactions on Sustainable Energy*. [CrossRef]

[8] Li, P. H., Jia, R., Cao, G., Ming, B., Guo, Y., Wang, S. K., & Li, W. (2025). A novel perspective for equivalent aggregation of wind farm: Measuring the dynamic similarity between output time-series. *Applied Energy*, *392*, 125958. [CrossRef]

[9] Yang, Y., Xu, Y., Gu, W., Mili, L., Sun, B., & Lu, S. (2025). A tensor-based clustering method for dynamic equivalent modeling of wind farms. *IEEE Transactions on Sustainable Energy*, *17*(2), 1075-1089, [CrossRef]

[10] Zhao, Z., & Chen, Z. (2026). Research on aggregated modeling of wind farms considering dynamic coupling characteristics and stability optimization in weak grid environments. *Strategic Planning for Energy and the Environment*, *45*(2), 403–428. [CrossRef]

[11] Teng, W., Wang, X., Meng, Y., & Shi, W. (2019).

An improved support vector clustering approach to dynamic aggregation of large wind farms. *CSEE Journal of Power and Energy Systems*, *5*(2), 215-223. [CrossRef]

[12] TingYun, G., HaoQian, G., Qiang, F., & ShuRan, Z. (2024, November). Modeling the equivalent of doubly fed wind turbine clusters using the K-means algorithm. In *2024 IEEE 8th Conference on Energy Internet and Energy System Integration (EI2)* (pp. 1296-1301). IEEE. [CrossRef]

[13] Cheng, J., Yan, T., Li, R., Meng, C., Tang, X., & Li, Z. (2023, November). KPCA-Based Hybrid Data-Model Driven Wind Farm Equivalence Modeling. In *2023 China Automation Congress (CAC)* (pp. 630-635). IEEE. [CrossRef]

[14] Rahman, M. T., Hasan, K. N., & Sokolowski, P. (2022). Evaluation of wind farm aggregation using probabilistic clustering algorithms for power system stability assessment. *Sustainable Energy, Grids and Networks*, *30*, 100678. [CrossRef]

[15] Gupta, A. P., Mitra, A., Mohapatra, A., & Singh, S. N. (2022). A multi-machine equivalent model of a wind farm considering LVRT characteristic and wake effect. *IEEE Transactions on Sustainable Energy*, *13*(3), 1396-1407. [CrossRef]

[16] Li, W., Chao, P., Liang, X., Ma, J., Xu, D., & Jin, X. (2017). A practical equivalent method for DFIG wind farms. *IEEE Transactions on Sustainable Energy*, *9*(2), 610-620. [CrossRef]

[17] Chao, P., Li, W., Liang, X., Xu, S., & Shuai, Y. (2021). An analytical two-machine equivalent method of DFIG-based wind power plants considering complete FRT processes. *IEEE Transactions on Power Systems*, *36*(4), 3657-3667. [CrossRef]

[18] Jin, Y., Wu, D., Ju, P., Rehtanz, C., Wu, F., & Pan, X. (2019). Modeling of wind speeds inside a wind farm with application to wind farm aggregate modeling considering LVRT characteristic. *IEEE transactions on energy conversion*, *35*(1), 508-519. [CrossRef]

[19] Zheng, Y., Wang, D., Zhou, Z., & Cao, T. (2014). Hierarchical protection control system of smart substations. *Journal of Modern Power Systems and Clean Energy*, *2*(3), 282-288. [CrossRef]

[20] Liu, Q., Li, M., Xu, J., & Jian, F. (2024, October). Model Simplification and Time Complexity Reducing Method For Security and Stability Control Systems. In *2024 IEEE PES 16th Asia-Pacific Power and Energy Engineering Conference (APPEEC)* (pp. 1-5). IEEE. [CrossRef]

[21] National Energy Administration. (2020). *Technical specification for design and application of power system safety and stability control system* (DL/T 2193-2020). Retrieved from https://www.chinesestandard.net/PDF/English.aspx/DLT2193-2020

[22] Liu, L., Li, L., Chen, B., Yu, H., Sun, W., Zhang, M., ... & Cheng, S. (2024, October). Aggregation Equivalence Method for New Energy Stations Based on PSASP Modelling Loss Consistency. In *2024 7th International Conference on Power and Energy Applications (ICPEA)* (pp. 668-673). IEEE. [CrossRef]

[23] General Administration of Quality Supervision, Inspection and Quarantine of the People's Republic of China, & Standardization Administration of China. (2011). *Technical rule for connecting wind farm to power system* (GB/T 19963-2011). Retrieved from https://www.codeofchina.com/standard/GBT19963-2011.html

[24] Lin, Y. L., Jiang, C. J., Ye, X. B., Zheng, J. H., & Xiahou, K. S. (2024, December). A combination of auxiliary circuits and reactive current control to improve low voltage crossing ability of offshore wind grid connection system. In *IET Conference Proceedings CP910* (Vol. 2024, No. 33, pp. 420-425). Stevenage, UK: The Institution of Engineering and Technology. [CrossRef]

[25] Lai, Q., Shen, C., & Li, D. (2024). Dynamic modeling and stability analysis for repeated LVRT process of wind turbine based on switched system theory. *IEEE Transactions on Power Systems*, *40*(3), 2711-2723. [CrossRef]

[26] Guo, Z., Fang, T., Liu, X., Zhao, Z., Yuan, B., & Wang, Y. (2025, August). Multi-Machine Equivalent Model for Impedance Analysis of Wind Farms. In *2025 5th Power System and Green Energy Conference (PSGEC)* (pp. 73-77). IEEE. [CrossRef]

[27] Brochu, J., Larose, C., & Gagnon, R. (2010). Validation of single-and multiple-machine equivalents for modeling wind power plants. *IEEE Transactions on Energy Conversion*, *26*(2), 532-541. [CrossRef]

[28] Zhou, X., Peng, J., Qi, J., Zhang, L., Zhu, Y., & Luo, C. (2025, April). Aggregate equivalent modeling of wind farm under full wind speed scenarios. In *2025 8th International Conference on Energy, Electrical and Power Engineering (CEEPE)* (pp. 448-453). IEEE. [CrossRef]

Xijian Dong received the M.S. degree in electrical engineering from Nanjing University of Aeronautics and Astronautics, Nanjing, China, in 2008. He is currently a Professor-Level Senior Engineer with the State Grid Corporation of China (SGCC) and serves as the Deputy Director of the System Protection Laboratory at NARI Group, SGCC. He is an Assistant Secretary of IEC SC8C (Network Management in Interconnected Electric Power Systems) and an active expert in Working Group 3 (WG3) on power system stability and security in planning, design, operation, and control. His research interests include power system security and stability control, as well as hardware-in-the-loop experiment technology for control systems. He has contributed to the formulation of two promulgated international standards, three electric power industry standards, and twelve SGCC enterprise standards. (Email: dong_xijian@163.com)

Jialong Wu received the M.S. degree from Beijing Jiaotong University, Beijing, China, in 2012. He is currently a Senior Engineer and a Master's Supervisor at the State Grid Electric Power Research Institute (NARI Group). His research interests include high-proportion renewable energy power system simulation and modeling, wide-band oscillation control, and experimental verification of stability control systems. He has served as a project leader or principal researcher for 2 national projects and 10 State Grid Corporation-level projects. He has published over 10 papers in core journals as the first or corresponding author and holds more than 10 authorized national invention patents.(Email:723852723@qq.com)

Yuqi Ma received the B.S. degree from Nanjing Tech University, Nanjing, China, in 2023, and the M.S. degree from State Grid Electric Power Research Institute, Nanjing, China, in 2026. She is currently an engineer at State Grid Electric Power Research Institute (NARI Group). Her research interests include modeling and simulation analysis of power systems with a high proportion of new energy.(Email: 2803646398@qq.com)

Jiaqi Feng received the B.S. degree from Nanjing Tech University, Nanjing, China, in 2019, and the M.S. degree from Nanjing Normal University, Nanjing, China, in 2026. He is currently an engineer at State Grid Electric Power Research Institute (NARI Group). His research interests include power grid security and stability control technology under high penetration of renewable energy. (Email: fengjiaqi@sgepri.sgcc.com.cn)

Yajie Li received the B.S. degree from Nanjing University of Posts and Telecommunications, Nanjing, China, in 2019, and the M.S. degree from Nanjing University of Science and Technology, Nanjing, China, in 2022. He is currently with China Electric Power Research Institute (NARI Group Corporation), Nanjing, China. His research interests include power system voltage stability analysis and operation and control of HVDC transmission systems. (Email: liyajie@sgepri.sgcc.com.cn)

Ming Lei received the B.S. degree from Sichuan University and the M.S. degree from Wuhan University, China, in 2006 and 2008, respectively. He is currently a Senior Engineer at State Grid Electric Power Research Institute, Nanjing, China. His research interests include modeling and simulation analysis of power systems, and applications of artificial intelligence in large power grids. He has published several papers. (Email: leiming1@sgepri.sgcc.com.cn)

Kui Deng received the M.S. degree from Chongqing University, Chongqing, China, in 2021. He is currently an engineer at State Grid Electric Power Research Institute (NARI Group), Nanjing, China. His research interests include modeling and simulation of new energy systems. (Email: dengkui@sgepri.sgcc.com.cn)